Prediction of spring Elbe discharge based on stable teleconnections with winter global temperature and precipitation

Monica Ionita

Alfred Wegener Institute for Polar and Marine Research, Bremerhaven, Germany

Gerrit Lohmann

Alfred Wegener Institute for Polar and Marine Research, Bremerhaven, Germany

DFG Research Centre for Ocean Margins, University of Bremen, Bremen, Germany

Norel Rimbu

Alfred Wegener Institute for Polar and Marine Research, Bremerhaven, Germany

Corresponding author:

Monica Ionita

Email: Monica.Ionita@awi.de

Address: Alfred Wegener Institute

Bussestrasse 24

D-27570 Bremerhaven

Germany

Telephone: +49(471)4831-1845

Abstract

We examine the predictability of Elbe streamflow anomalies during spring using previous winter sea surface temperature (SST), temperature over land (TT) and precipitation (PP) anomalies. Based on running correlation analysis, we identify several regions where the spring streamflow anomalies are stable correlated with SST, TT and PP anomalies from previous winter. We show that during the period 1902-1971 the Elbe spring streamflow is stable correlated with previous winter PP anomalies from its catchment area, with TT anomalies from the Black Sea-Caspian Sea region, north-western Europe and northern Canada, as well as with SST anomalies from the tropical Pacific, the Indian Ocean and several regions of the North Pacific and the North Atlantic. An index based on winter SST, TT and PP anomalies from these regions is highly significantly correlated with spring streamflow anomalies during this period. Based on SST, TT and PP anomalies from stable correlated regions, a forecast scheme is developed and applied to predict spring streamflow anomalies during the last decades. The prediction based on our statistical scheme represents a marked improvement relative to the forecast based on teleconnection indices which are traditionally used for streamflow prediction.

1. Introduction

One of the most difficult issues of hydrology is how to appreciate the seasonal variability of rivers discharge. Water is a vital resource for human as well as natural ecosystems. It has been established that changes in the cycling of water between land, sea and air can have significant impacts on the environment, economy and society through their effects on the water resources and their management (Arnell, 1995, 1999; Arnell and Reynard, 1996). The availability of water is greatly influenced by climate conditions that vary on seasonal, interannual, and decadal time scales. Characterisation of hydrological variability on climatic timescales and identification of connections to climate forcings provide potential improvement for hydrological forecasts when these forcings are predictable or slowly evolving (Souza and Lall, 2003; Croley, 2003).

Over the last years, interest in seasonal predictability of river discharge variability over Europe has increased markedly (Trigo et al., 2004; Rimbu et al., 2004; Rimbu et al., 2005). On seasonal timescales, anomalous atmospheric conditions are often linked with seasonal variations in the rivers streamflow, via variations in precipitation and temperature (Dettinger and Diaz, 2000; Cullen et al., 2002). For example, spring and summer rainfall and temperature anomalies across Europe may be forecasted from prior knowledge of varying boundary conditions such as anomalous sea surface temperature in the North Atlantic (Colman, 1997; Colman and Davey, 1999; Wilby, 2001) and/or the tropical Pacific (Kiladis and Diaz, 1989; Lloyd-Hughes and Saunders, 2002; van Oldenborgh et al., 2000). Spring precipitation over central Europe is higher than normal average following warm El Niño events combined with lower SSTs west of Ireland (Lloyd-Hughes and Saunders, 2002). Predictability is found to be higher in El Niño-Southern Oscillation (ENSO) extreme years

(Branković and Palmer, 2000), implying that at least part of the available skill can be attributed to the forcing from the tropical Pacific Ocean.

Two of the most important phenomena that influence streamflow variability are the North Atlantic Oscillation (NAO) and ENSO (Dettinger and Diaz, 2000; Cullen et al., 2002). The indices of these large-scale climatic patterns are used as predictors for seasonal streamflow anomalies over Europe (Rimbu et al., 2005, Cullen et al, 2002, Trigo et al., 2004). Significant lag-correlations were identified between NAO index and several river streamflow anomalies from the Iberian Peninsula (Trigo et al., 2004) and Tigris-Euphrates streamflow anomalies (Cullen et al., 2002). Rimbu et al. (2004) found significant lag-correlation between NAO and ENSO indices and Danube streamflow. However, the association between NAO and ENSO and streamflow from the Iberian Peninsula (Trigo et al., 2004) and from south-east Europe (Rimbu et al., 2004; Cullen et al., 2000) is non-stationary, i.e. the strength of the correlation between these two phenomena and streamflow anomalies has changed over time. These teleconnection patterns, though dominant on a large scale, often fail to provide forecast skill in individual basins (McCabe and Dettinger, 2002; Grantz et al, 2005). The predictability of precipitation and streamflow from Europe using NAO and ENSO as predictors is limited due to non-stationarity. One way to improve the seasonal forecast for streamflow would be to identify stable predictors.

This paper describes a forecasting scheme for spring Elbe streamflow based on stable lag-correlation with temperature and precipitation indices. It is shown that when climate indices from key regions are used together as predictors, the forecast improves compared to the case when they are used separately.

The present study is structured as follows. In section 2 we describe the data sets and methods used in this paper. In section 3 the main results are presented. The main conclusions and a discussion follow in section 4.

2. Data and methodology

2.1 Data sets description

The Elbe rises at an elevation of about 1400 m in the *Giant Mountains* on the north-west border of the Czech Republic. It is approximately 1.100 km long and covers a catchment area of about 150.000 km² that is inhabited by 25 million people. It passes through the Czech Republic and Germany and discharges into the German Bight, North Sea (Figure 1, this picture is placed at the disposal of the Potsdam Institute for Climate Impact Research and River Basin Community Elbe). The monthly time series of Elbe discharge, used in this paper, were recorded at Neu Darchau (53° 14′ N, 10° 53′ E), which is situated in the lower part of the Elbe catchment area (last gauging station), and they were provided by the German Federal Institute of Hydrology (BfG) in Koblenz, Germany. The hydrological discharge regime is characterized by a pronounced seasonal cycle the rising limb of which is situated between January and April and the falling one between June and September, the highest values being recorded in April. These high discharge values recorded in the spring months may be related with the melting of the snow in the catchment area and the soil humidity.

Taking into account that the highest discharge values are recorded in the spring season (Figure 2-upper right), we focused our analysis on this specific season (March/April/May). The spring Elbe streamflow for the period 1902-2001 is presented in Figure 2. It shows strong interannual and decadal variations. The strongest positive discharge anomaly during the analyzed period occurred in the 1940-1942, a period dominated by strong climate anomalies (Brönnimann et al., 2004; Brönnimann, 2007).

From the monthly time series we computed the seasonal spring mean, by averaging the months March/April/May (MAM). From the seasonal means we calculate the seasonal anomalies against the mean over the period 1902-2001. The time series was detrended and

normalized by the corresponding standard deviation to obtain normalized anomalies of Elbe streamflow for MAM.

As predictors we used the following data sets:

a) The SST was taken from the Kaplan data set (Kaplan et al., 1998). This data set has a resolution of 5ºlat x 5ºlon and covers the period 1901-2001. We used the winter SST field - December/January/February (DJF). The time series were detrended and normalized by the corresponding standard deviation to obtain normalized anomalies of SST for DJF.

b) The temperature (TT) and precipitation (PP) was taken from CRU (Climatic Research Unit) TS2.1 data set (Mitchell et al., 2003). The data sets have a 0.5º x 0.5º horizontal resolution and cover the period 1902-2001. The same data processing was used as for SST.

c) We also used the time series of the monthly teleconnection indices described in Table I. The seasonal values of these indices were calculated using the same methodology as for the Elbe streamflow data, but for the winter season (DJF).

Large-scale sea level pressure (SLP) patterns associated to the river streamflow variability are based on the updated version of the SLP data set constructed by Trenberth and Paolino (1980). This data set has a 5ºlat x 5ºlon resolution.

2.2 Methodology

For the forecast scheme all the data sets were separated into two parts: a) the calibration period (1902-1971) and b) the validation period (1972-2001).

The forecast scheme for seasonal prediction of spring Elbe streamflow anomalies using SST, TT and PP from previous winter is based on a methodology similar to that used for seasonal prediction of Danube streamflow (Rimbu et al., 2005). The basic idea of this scheme is to use SST, TT and PP anomalies from regions with stable teleconnections as predictors (Lohmann

et al., 2005). However, in our study we have used a different criterion to define the stability of the correlation (Lohmann et al., 2005) and we added new predictors, i.e. the anomalies of TT and PP over land, comparative with previous studies (Rimbu et al., 2005). We correlate the spring streamflow anomalies with global SST, TT and PP anomalies from previous winter in a moving window of 31 years. The correlation is considered to be stable for those grid-points where spring streamflow and winter SST, TT or PP anomalies are significantly correlated at 90% level (r=0.24) or 80% level (r=0.17) for more than 80% of the 31-year windows covering the period 1902-2002. The regions where correlation is positive and stable at 90% (80%) level will be represented as red (orange) on a global map. The regions where correlation is negative and stable at 90% (80%) level will be represented as blue (violet). Such maps will be referred to in our study as stability correlation maps. The stability correlation maps derived in our study remain qualitatively the same if the significance levels that define the stability of the correlation vary within reasonable limits.

To better understand how the correlation stability maps are constructed we present as an example the decadal variation of the correlation between spring Elbe streamflow and SST anomalies from several grid points (Figure 3). The spring streamflow and winter SST from (140.5°W, 10.5°N) grid point are positively correlated for all 31-year windows covering the period 1901-2002 and above the 90% significant level for more than 80% windows. The streamflow and SST from the grid point (70.5°E, 5.5°N) is positive and above 80% significance level for more than 80% windows (Figure 3). Therefore, these grid points are stable correlated with streamflow and are represented on the stability map of correlation as red and orange, respectively (Figure 4). The spring streamflow and SST from the grid points (70.5°W, 30.5°N) and (170.5°E, 40.5°N) are negative and above 90% and 80% significance level, respectively, for more than 80% windows. Also these grid points are stable correlated with streamflow and are represented on the stability correlation map as blue and violet,

respectively (Figure 4). On the contrary, the streamflow and SST from the grid point (55.5°W, 10.5°N) are significantly correlated for less than 80% windows, and therefore the correlation is unstable according to our criteria. Such a grid point appears in white colour on the stability map of correlation (Figure 4).

2.3 Model evaluation

Several methods are common to assess the skill of forecast models (i.e. Wilks, 1995; von Storch and Zwiers, 1999). We employ the percentage improvement in the root-mean-square error over a climatological forecast ($RMSE_{cl}$) and over persistence ($RMSE_{per}$). The RMSE skill measure is one of the most robust. Climatology is taken as the standardized long-term average prior to each year being forecasted, while persistence is taken as winter (DJF) Elbe streamflow standardized anomalies. We computed the skill score S (Wilks, 1999), defined as:

$S = 1 - \frac{RMSE(forecast)}{RMSE(reference\ forecast)}$, where the reference forecast is either climatology or persistence.

The skill score is one for perfect forecasts, zero for forecasts no better than the reference forecast and is unbounded below zero for forecasts that are worse than the reference forecast.

3. Stable teleconnections of the Elbe streamflow

a. Sea surface temperature

The stability correlation map between spring streamflow and winter SST (Figure 4a) emphasizes several stable regions during the period 1902-1971. The spring streamflow is stable correlated with winter SST anomalies from parts of the central and eastern Pacific, several regions of the North Atlantic, the west coast of Europe, the eastern Mediterranean and

the Red Sea. Consistent with this result, significant positive correlations between ENSO indices and river flow from Europe (Dettinger and Diaz, 2000; Rimbu et al., 2004) as well as precipitation over Europe (Mariotti et al., 2002) were identified.

We consider that the SST anomalies from these regions represent stable predictors for Elbe spring streamflow anomalies. Based on the stability map we defined 9 SST indices by averaging the normalized SST anomalies for the regions described in Table II (first column). The first EOF of these indices (Figure 4b) which explains 33.39% of the total variance has a spatial structure consistent with the SST pattern identified in the stability map. The correlation between the first time coefficient (PC1) associated to EOF1 and spring streamflow anomalies for a 31-year moving window (Figure 4c - upper part), for the period 1902-1971, is significant at 95% level (following the t-test). The time series of PC1 shows variations similar with Elbe spring streamflow for the same period (Figure 4c-lower part). The correlation between the two time series, over the entire period (1902-1971) is r= +0.56 and is significant at 95% level.

The highest values of spring Elbe discharge during the period 1901 to 2002 are recorded in 1941 (Figure 2) which is well predicted by PC1 of winter SST indices as defined above (Figure 4c). This strong positive discharge anomaly can be related to the very strong El Niño event, developing in that period (Brönnimann et al., 2004). Indeed, the SST anomaly map for the 1940/41 winter (Figure 5a) shows strong anomalies in the regions stably correlated with spring streamflow (Figure 4). Besides a strong Pacific-North American pattern that accompanies this El Niño event, significant positive sea level pressure anomalies are recorded in the Iceland region as well as negative sea level pressure anomalies over central and eastern Europe including the Elbe region (Figure 5b). Such a circulation pattern is consistent with high winter precipitation anomalies over the Elbe catchment area during

winter. These winter precipitation anomalies, which partly can be snow or ice, are likely to be responsible for the positive streamflow anomalies recorded in spring 1941.

b. Surface temperature over land

The stability correlation map between spring streamflow and winter TT (Figure 6a) shows stable regions in the Amazonian domain, the northern part of Canada, the central and northern part of Europe, the Middle East and a small part of Siberia. The TT correlation pattern associated with spring streamflow in the Northern Hemisphere projects well on the corresponding pattern associated with NAO, consistent with a strong influence of winter NAO on spring streamflow anomalies in the Europe (Dettinger and Diaz, 2000; Trigo et al., 2004). However, from Figure 6a we can see that spring Elbe streamflow is stable correlated not only with NAO-related TT anomalies but also with TT anomalies from other regions. This suggests that other winter phenomena, not necessarily related with NAO, influence the spring streamflow anomalies also. For example, the stable correlation pattern from the northeastern part of South America could be related to ENSO (Marengo, 1992; Ronchail et al, 2002), while those from northern North America could be connected with winter snow cover anomalies (Sobolowski et al., 2007).

Based on the stability map, we defined 6 TT indices by averaging the normalized TT anomalies for the regions described in Table II (second column). The first EOF computed on the basis of the indices defined above (Figure 6b), which explains 40.20% of the total variance, has a structure coherent with the stability map. The correlation between the first time coefficient (PC1) associated to EOF1 and spring streamflow anomalies for a 31-year moving window (Figure 6c - upper part), for the period 1902-1971, is also significant at 95% level. The time series of PC1 and ELBE spring streamflow is shown in Figure 6c (lower

part). The correlation between the two time series, over the entire period, is r= +0.54 (significant at 95% level).

c. Precipitation

For precipitation we identified just one significant stable region (Figure 7a), which covers most of the central and south Europe. The stable correlation between winter PP anomalies from this region and spring streamflow anomalies of Elbe river is consistent with the strong relationship between PP anomalies and river discharge over Europe (Dettinger and Diaz, 2000). However the region of stable correlation is extended over a broad region of central and Eastern Europe (Figure 7a). The PP anomalies outside the catchment area are not necessarily directly related to spring streamflow anomalies. They can be related to SST or TT anomalies from the regions stably related with spring streamflow anomalies (Figures 4 and 6). There are also some stable grid points over the west coast of the U.S., but we will focus just on the European region.

The correlation coefficient for a 31-year moving window between MAM streamflow and a precipitation index, defined on the region (0.5ºE-45.5ºE; 40.5ºN-50.5ºN), is shown in Figure 7b. The correlation coefficient between MAM streamflow and PP index is r= +0.50 during the period 1902-1971.

d. Combination of indices

To identify the most skilful predictors when considering the forecast scheme, we computed the EOF, taking into account all the indices defined above (SST+TT+PP). Beside the EOF analysis we also tried to develop a forecast model based on linear regression (not shown). We

used a step-wise regression model in order to identify the optimal number of indices to be used for the flow prediction. Taking into account that the results using the EOF analysis and the ones obtained using regression were almost similar, we have decided to present just the results for the EOF analysis.

The first EOF (Figure 8a) explains 35.05% of the total variance. The correlation coefficient for the 31-year moving window between the first time coefficient (PC1) corresponding to EOF1 and MAM streamflow is higher than when considering each index separately (Figure 8b). The correlation coefficient for the 31 years running window is significant at 95% level, in contrast with the correlation between spring streamflow and winter NAO and NINO indices. The correlation coefficient between spring streamflow and PC1 is 0.59 (Figure 8b-lower panel), which is higher than when we considered each predictor separately. The correlation coefficient between spring streamflow and winter NAO (NINO3) index, over the same period, is -0.27 (0.26). Furthermore, the PC1 is also a better predictor than previous winter Elbe discharge (Figure 8b - upper panel). We can conclude that PC1 is a better predictor for spring streamflow than winter NAO and Niño3 indices as well as previous winter Elbe discharge, especially when considering SST+TT+PP indices together.

Taking into account that other teleconnection patterns have also been found to have an important impact on the precipitation variability in the European region, we computed the correlation, in a 31-year window, between Elbe spring anomalies and other teleconnection indices from the North Atlantic region, such as East Atlantic, East Atlantic/Western Russia, Scandinavian and Polar/Eurasian patterns (Barnston and Livezey, 1987). The influence of these teleconnection patterns on the variability of precipitation and temperature in different regions in Europe was emphasized in different studies (Slonosky et al., 2001, Goodes and Jones, 2002; Martin et al., 2004; Rodriguez-Puebla et al., 2001; Trigo et al., 2006).

The correlation coefficients between Elbe streamflow and the winter time series of these teleconnection indices are shown in Figure 9. For this analysis we used just the period 1950-2001, due to the lack of data before 1950. Like in the case of NAO and NINO3, the correlation is much smaller when compared to PC1. One reason that could explain this is that these teleconnection patterns have weak projection on the precipitation field over the Elbe catchment area.

e. Potential predictability

Rimbu et al. (2005) showed that prediction based on SST identified in stable key regions improves compared to prediction based on NAO and ENSO indices.

Assuming that the regions of stable teleconnections established for the period 1902-1971 do not change significantly for the period 1972-2001, we calculate the SST, TT and PP indices for the region defined above and the corresponding PC1 successively, using the data from 1902-1972, 1902-1973….to 1902-2001. The last values of PC1 based on these updated winter SST, TT and PP indices, represent the streamflow anomaly forecast for the next spring. The result of the forecast is represented in Figure 10. The predicted and observed spring streamflow anomalies are significantly correlated (**r = 0.63**). The correlation between predicted spring streamflow anomalies based on winter NAO and Niño3 indices is **-0.16** and **0.17**, respectively. Therefore, the prediction based on our statistical scheme is a marked improvement compared to prediction based only on NAO and Niño3 indices.

To better asses the skill of the forecast, we made use of the RMSE and the skill score (Wilks, 1995). The results of this analysis are shown in Table III. From Table III, it can be seen that although our forecast model is not very accurate, it does exhibit a useful skill that is approximately 20% better than both climatology and persistence. In the case of NAO and

Niño3, the skill score shows negative values, which implies that the forecast based on them has less accuracy than climatology or persistence.

4. Discussions and conclusions

We have investigated the predictability of spring Elbe streamflow anomalies, using SST, TT and PP anomalies from previous winters as predictors. It appears that the teleconnections with SST, TT and PP are stable over various regions of the globe. Large areas in the central Pacific, North Atlantic, extending to the Red Sea, of winter SST anomalies area are stable correlated with Elbe spring streamflow, which is consistent with previous studies related to the impact of SST anomalies on European climate (Dettinger and Diaz, 2000; Marrioti et al., 2002; Rimbu et al., 2004; Rimbu et al., 2005). Several key regions where MAM streamflow is stably correlated were also identified in the global TT field. Key regions from the northern part of Canada, the Amazonian region, Europe, the Middle East and a small part of Siberia are stably correlated with MAM streamflow. For precipitation the most stable region is the central and northern part of Europe. Therefore, the spring Elbe streamflow anomalies are related not only with regional winter climatic anomalies but also with climate anomalies from several key regions located far from Elbe region. We have shown that the forecast skill improves when these remote predictors are considered in the forecast scheme.

The signal to noise ratio was increased by deriving the first EOF of the SST, TT and PP indices calculated over the stable regions. The corresponding time series (PC1) is then used as a predictor for the streamflow anomalies. We also found that the correlation coefficient increases when we calculate the EOF using all the indices (SST+TT+PP), comparing to the case when we make the analysis separately on each of them. It has been also found that the

prediction of spring streamflow anomalies based on the method described above is better than the prediction based on NAO and ENSO.

Winter precipitation in central Europe is mainly influenced by cyclonic activity, carried by the dominant westerlies. During winter season the dominant patterns of climate variability over Europe which produces significant precipitation anomalies are NAO and ENSO (Mariotti et al., 2002; Cullen et al., 2002). However, the impact of ENSO on European climate could be dependent on the strength of the ENSO anomalies (van Loon and Madden, 1981) or on the phases of ENSO. Pozo-Vazquez et al. (2005) showed that the impact of La Niña events on European climate is stronger than the impact of El Niño events. Strong La Niña events during autumn give a detectable signal in winter precipitation over Europe. Such winter precipitation anomalies are likely recorded as Elbe streamflow anomalies in the next spring, consistent with the stable correlation between spring streamflow anomalies and winter precipitation.

The enhanced predictability of spring streamflow can be also related to the relatively high predictability of spring precipitation from winter SST as discussed in recent studies (Oldenborgh et al., 2000; Knipertz et al., 2003). Predictability is found to be higher in El Niño-Southern Oscillation extreme years (Branković and Palmer, 2000), implying that at least part of the available skill can be attributed to the forcing from the tropical Pacific Ocean. Merkel and Latif (2002) suggested that an El Niño-related weakening of the North Atlantic mean meridional pressure gradient and a southward shift of the North Atlantic stormtrack induce wetter conditions over central Europe and the western Mediterranean and colder temperatures over Scandinavia.

Our analysis shows that winter SST, TT and PP anomalies from several key regions provide a significant source of predictability for Elbe spring streamflow. Also a small, but significant

potential predictability was detected for summer streamflow anomalies using previous spring SST, TT and PP anomalies from several key regions.

Our forecast scheme shows an improvement of about 20% when compared with climatology and persistence and major advantages than the forecast based on different teleconnection patterns.

We argue that a skilful prediction, based on stable teleconnections can provide guidance for water management in the Elbe river catchment area, with consequences for economy, agriculture and hydroelectricity.

Acknowledgments. The authors are grateful to Dr. Mihai Dima for providing thoughtful comments. Thanks are due to the German Federal Institute of Hydrology (BfG) for supplying the data sets for Elbe river discharge.

References

Arnell, N.W., 1995: Scenarios for hydrological climate change impact studies. In The Role of Water and the Hydrological Cycle in Global Change, Oliver HR, Oliver S (eds). NATO ASI Series 1, *Springer-Verlag: Berlin*, Heidelberg, vol. 31., 393–396.

Arnell, N.W., 1999: The effect of climate change on hydrological regimes in Europe: a continental perspective. *Global Environmental Change,* **9,** 5–23.

Arnell, N.W., and N.S. Reynard, 1996. The effects of climate change due to global warming on river flows in Great Britain. *J. Hydrol.,* **183**, 397–424.

Barnston, A.G., and R.E. Livezey, 1987: Classification, seasonality and persistence of low frequency atmospheric circulation patterns. *Mon. Wea. Rev.*, **115**, 1083–1126.

Branković, C., T.N. Palmer, and L. Ferranti, 1994: Predictability of seasonal atmospheric variation. *J. Climate,* **7**, 217–237.

Brönnimann, S., J. Luterbacher, J. Staehelin, T.M. Svenby, G. Hansen, and T. Svenoe, 2004: Extreme climate of the global troposphere and stratosphere 1940-1942 related to El Nino. *Nature*, **431**, 971-974.

Brönnimann, S., 2007: Impact of El Niño–Southern Oscillation on European climate. *Rev. Geophys.*, **45**, RG3003, doi:10.1029/2006RG000199.

Colman, A., 1997: Prediction of summer Central England Temperature from preceding North Atlantic winter sea surface temperature. *Intl. J. Climatol.,* **17**, 1285–1300.

Colman, A., and M. Davey, 1999: Prediction of summer temperature, precipitation and pressure in Europe from preceding winter North Atlantic Ocean temperature. *Intl. J. Climatol.*, **19**, 513–536.

Croley, T.E. II, 2003: Great Lakes climate change hydrologic impact assessment I.J.C. Lake Ontario-St. Lawrence River Regulation Study. NOAA Technical Memorandum GLERL, **126**, 77 pp.

Cullen, H.M., A. Kaplan, P. Arkin, and P.B. DeMenocal, 2002: Impact of the North Atlantic Oscillation on Middle Eastern climate and streamflow. *Clim. Change*, **55**, 315– 338.

Dettinger, M.D., and H.F. Diaz, 2000: Global characteristics of streamflow seasonality. *J. Hydrometeor.*, **1**, 289– 310.

Goodess, C.M., and P.D. Jones, 2002: Links between circulation and changes in the characteristics of Iberian rainfall. *Intl. J. Climatol.*, **22**, 1593-1615.

Grantz, K., B. Rajagopalan, M. Clark, and E. Zagona, 2005: A technique for incorporating large-scale climate information in basin-scale ensemble streamflow forecasts, *Water Resour. Res.*, **41**, W10410, doi:10.1029/2004WR003467

Jones, P.D., T. Jonsson, and D. Wheeler, 1997: Extension to the North Atlantic Oscillation using early instrumental pressure observations from Gibraltar and South-West Iceland. *Intl. J. Climatol.*, **17**, 1433– 1450.

Kaplan A, M.A. Cane, Y. Kushnir, A.C. Clement, M.B. Blumenthal, and B. Rajagopalan, 1998: Analyses of global sea surface temperature 1856–1991. *J. Geophys. Res.,* **9**, 18 567–18 589.

Kiladis, G.N., and H.F. Diaz, 1989: Global climatic anomalies associated with extremes in the Southern Oscillation. *J. Climate,* **2**, 1069–1090.

Knippertz, P., U. Ulbrich, F. Marques, and J. Corte-Real, 2003: Decadal changes in the link between El Niño and spring North Atlantic oscillation and European-North African rainfall. *Intl. J. Climatol.*, **23**, 1293– 1311.

Lloyd-Hughes, B., and M.A. Saunders, 2002: Seasonal prediction of European spring precipitation from ENSO and local sea surface temperatures. *Intl. J. Climatol.*, **22,** 1–14.

Lohmann, G., N. Rimbu, and M. Dima, 2005: Where can the Arctic Oscillation be reconstructed? Towards a reconstruction of climate modes based on stable teleconnections. *Clim. Past Disc.*, **1**, 17–56.

Marengo J.A, 1992: Interannual variability of surface climate in the Amazon basin. *Intl. J. Climatol.,* **12**, 853–863.

Mariotti, A., N. Zeng, and K.M. Lau, 2002: Euro-Mediterranean rainfall and ENSO - A seasonally varying relationship. *Geophys. Res. Lett.*, **29(12)**, 1621, doi:10.1029/2001GL014248.

Martin, M.L., Luna M.Y., Morata A., and Valero F., 2004: North Atlantic teleconnection patterns of low-frequency variability and their links with springtime precipitation in the western Mediterranean. *Intl. J. Climatol.*, **24**, 213-230.

McCabe, G.J., and M.D. Dettinger, 2002: Primary modes and predictability of year-to-year snowpack variation n the Western United States from teleconnections with Pacific Ocean Climate. *J. Hydrometeor.*, **3**, 13-25.

Merkel, U., and M. Latif, 2002: A high resolution AGCM study of El Niño impact on the North Atlantic/European sector. *Geophys. Res. Lett.*, **29(9)**, doi: 10.1029/2001GL013726

Mitchell, T.D., T.R. Carter, P.D. Jones, M. Hulme, and M. New, 2003: A comprehensive set of high-resolution grids of monthly climate for Europe and the globe: The observed record (1901-2000) and 16 scenarios (2001-2100). *Tyndall Center Working Paper*, **55**, available online at http://www.tyndall.ac.uk/publications/working_papers/wp55.pdf

Pozo-Vázquez, D., S.R. Gamiz-Fortis, J. Tovar-Pescador, M.J. Esteban-Parra, and Y. Castro-Diez, 2005: El Niño-Southern Oscillation events and associated European winter precipitation anomalies. *Intl. J. Climatol.,* **25**, 17–31.

Rimbu, N., M. Dima, G. Lohmann, and I. Musat, 2005: Seasonal prediction of Danube flow variability based on stable teleconnection with sea surface temperature. *Geophys. Res. Lett.*, **32**, L21704, doi:10.1029/2005GL024241.

Rimbu, N., M. Dima, G. Lohmann, and S. Stefan, 2004: Impacts on the North Atlantic Oscillation and the El Niño-Southern Oscillation on Danube river flow variability. *Geophys. Res. Lett.,* **31**, L23203, doi:10.1029/2004GL020559.

Rodríguez-Puebla, C., A.H. Encinas, and J. Sáenz, 2001: Winter precipitation over the Iberian peninsula and its relationships to circulation indices. *Hydrology and Earth System Sciences,* **5**, 233-244.

Ronchail, J., G. Cochonneau, M. Molinier, J. L. Guyot, A. Gorreti, V. Guimarães, and E. De Oliveira, 2002: Interannual rainfall variability in the Amazon Basin and sea surface temperatures in the equatorial Pacific and the tropical Atlantic Oceans. *Int. J. Climatol*., **22,** 1663–1686.

Sobolowski, S., G. Gong, and M. Ting, 2007: Northern Hemisphere winter climate variability: Response to North American snow cover anomalies and orography. *Geophys. Res. Lett.*, **34**, L16825, doi:10.1029/2007GL030573.

Slonosky, V.C., P.D. Jones, and T.D. Davies, 2001: Atmospheric circulation and surface temperature in Europe from the 18th century to 1995. *Int. J. Climatol*., **21**, 63-75.

Souza, F., and U. Lall, 2003: Seasonal to interannual ensemble streamflow forecasts for Ceara, Brazil: applications of a multivariate, semiparametric algorithm. *Water Resour. Res.,* **39**, 1–13.

Trenberth, K. E., and D. A. Paolino, 1980: The Northern Hemisphere sea-level pressure data set: Trends, errors and discontinuities. *Mon. Wea. Rev.* **108**, 855-872.

Trigo, R.M., D. Pozo-Vázquez, T.J. Osborn, Y. Castro-Diez, S. Gamiz-Fortis, and M.J. Esteban-Parra, 2004: North Atlantic Oscillation influence on precipitation, river flow and water resources in the Iberian Peninsula. *Int. J. Climatol*., **24**, 925–944.

Trigo, R.M., 2006: Relations between variability in the Mediterranean region and mid-latitude variability. In *Mediterranean Climate Variability; Developments in Earth & Environmental Sciences* 4, Elsevier, pp 179-226.

van Loon, H., and R. Madden, 1981: The Southern Oscillation. Part I: Global associations with pressure and temperature in northern winter. *Mon. Wea. Rev.,* **109**, 1150–1162.

van Oldenborgh, G.J., G. Burgers, and A. Klein Tank, 2000: On the El Niño teleconnection to spring precipitation in Europe. *Int. J. Climatol*., **20**, 565–574.

von Storch H, and F Zwiers, 1999: Statistical Analysis in Climate Research. *Cambridge University Press*, 494 pp.

Wilby, R.L., 2001: Downscaling summer rainfall in the UK from North Atlantic Ocean temperatures. *Hydrology and Earth Systems Sciences,* **5**, 245–257.

Wilks, D.S., 1995: Statistical Methods in the Atmospheric Sciences. *International Geophysics Series*, Vol. 59, Academic Press, San Diego, pp. 464.

Figure captions

Figure 1. The Elbe catchment area.

Figure 2. The time series of MAM Elbe discharge recorded at Neu Darchau (53° 14′ N, 10° 53′ E) for the period 1902-2001 and the seasonal mean discharge of Elbe (upper-right). Units are $m^3s^{-1.}$

Figure3. Running correlation (31 year window) between spring flow and winter SST anomalies from the grid points indicated in the upper-right corner of the figure. The correlation is plotted at the beginning of each 31-year window. The first points represent the correlation between spring flow from 1902-1933 and SST from 1901/1902-1932/1933.

Figure 4. a) The stability map of the correlation between spring flow and winter SST anomalies. Regions where the correlation is stable, positive and significant at 90% (80%) level for at least 80% windows are shaded with red (orange). The corresponding regions where the correlation is stable but negative are shaded with blue (violet). b) First EOF of the SST indices (see Table II for definition). c) Running correlation (31 year window) between spring flow and PC1 of SST indices (upper panel) and spring flow anomalies (grey line) and PC1 (dark line) of winter SST from stable regions.

Figure 5. a) Sea surface temperature anomalies and b) sea level pressure anomalies for the winter 1940/41. Units ºC and hPa.

Figure 6. As in figure 4, but for TT

Figure 7. a) The stability map of the correlation between spring flow and winter PP anomalies. Regions with stable correlations are shaded. b) Running correlation (31 year window) between spring flow and PP index (see Table II for definition) (upper panel) and spring flow anomalies (grey line) and winter PP index (dark line) from the stable region.

Figure 8. a) First EOF of the (SST+TT+PP) indices identified in Figures 4, 6 and 7 (see Table II for definition). b) Running correlation (31 year window) between spring flow and PC1 of (SST+TT+PP) indices (black line), NAO index (light dashed grey line), Niño3 index (dark dotted grey line) and winter flow anomalies (light grey line). c) The time series of PC1 (dark line) of winter (SST+TT+PP) from the stable regions and spring flow anomalies (grey line).

Figure 9. Running correlation (31 year window) between spring flow and teleconnection indices from the North Atlantic region.

Figure 10. Observed (back line) and predicted (grey line) spring flow anomalies for the period 1972-2001 based on winter (SST+TT+PP) anomalies from the stable regions.

Figure 1. The Elbe catchment area.

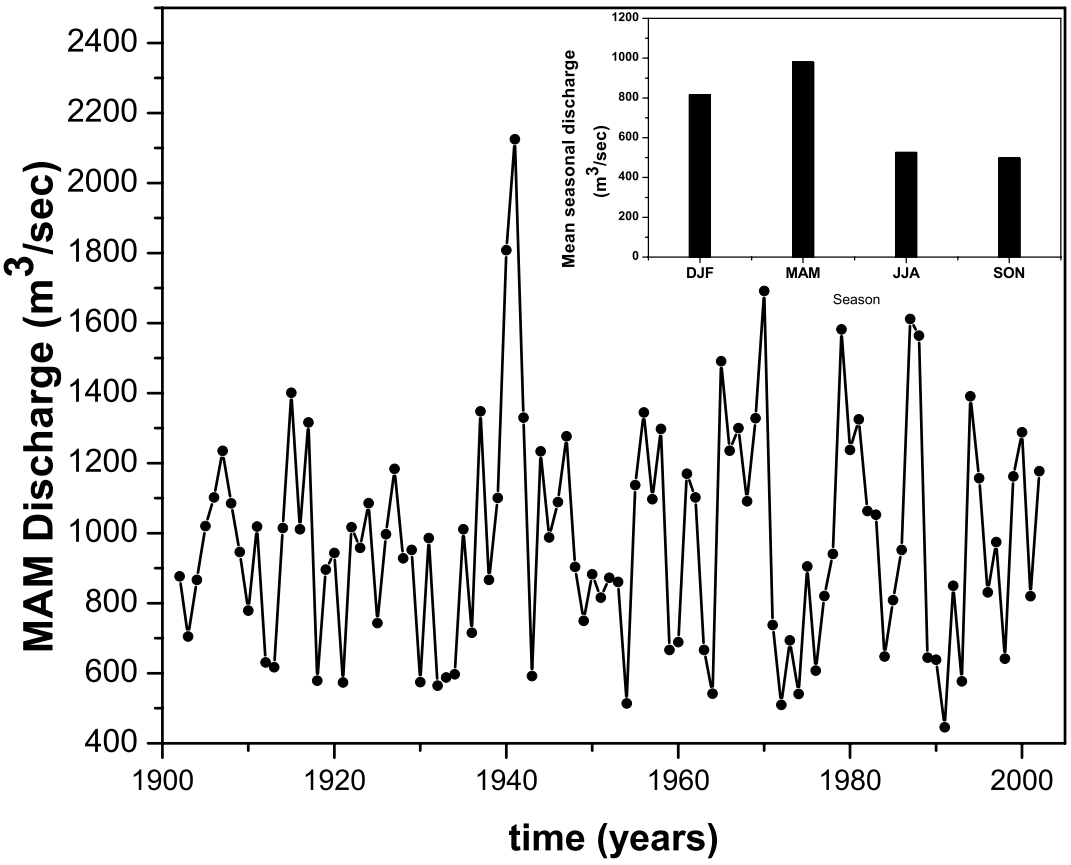

Figure 2. The time series of MAM Elbe discharge recorded at Neu Darchau (53° 14′ N, 10° 53′ E) for the period 1902-2001 and the seasonal mean discharge of Elbe (upper-right). Units are m^3s^{-1}.

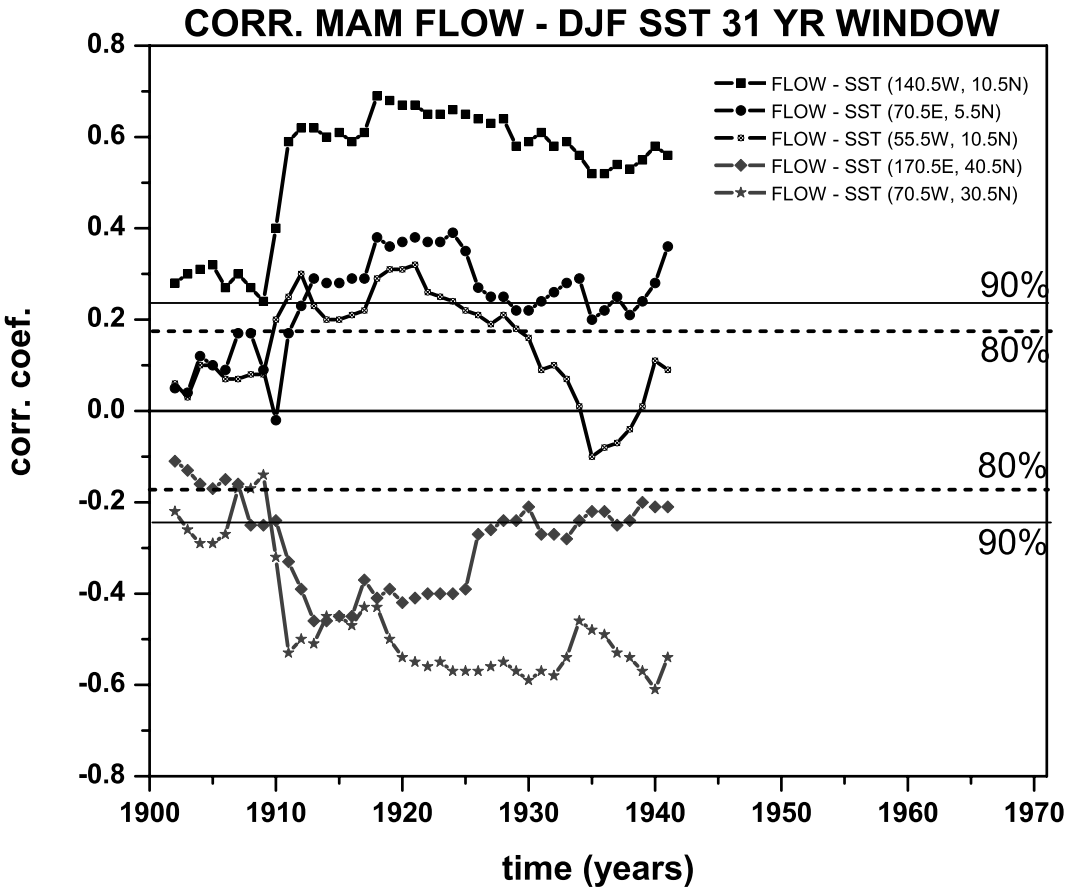

Figure3. Running correlation (31 year window) between spring flow and winter SST anomalies from the grid points indicated in the upper-right corner of the figure. The correlation is plotted at the beginning of each 31-year window. The first points represent the correlation between spring flow from 1902-1933 and SST from 1901/1902-1932/1933.

a)

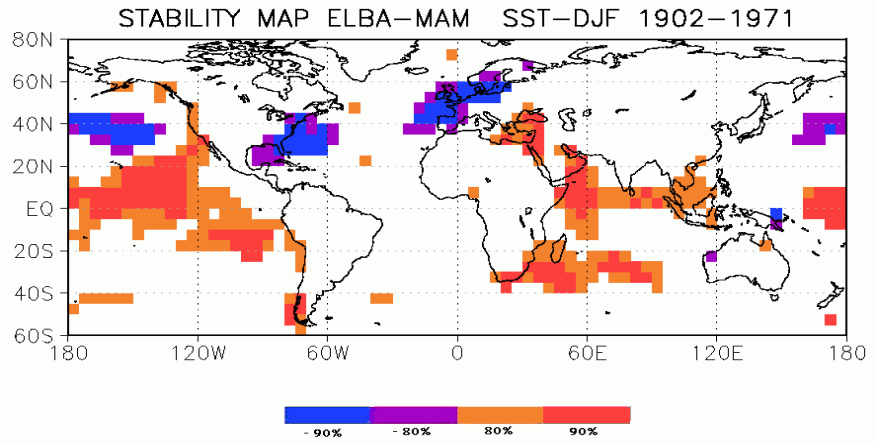

b)

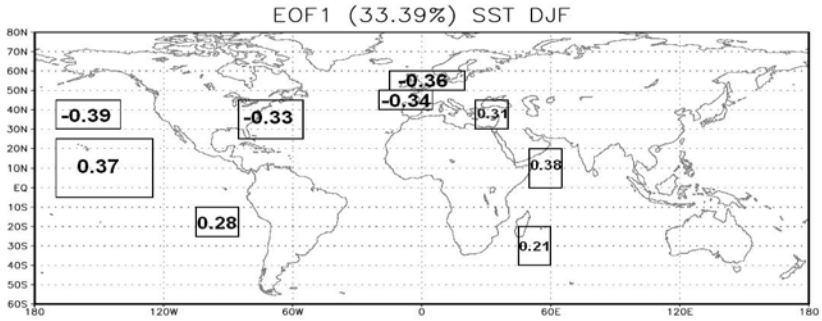

c)

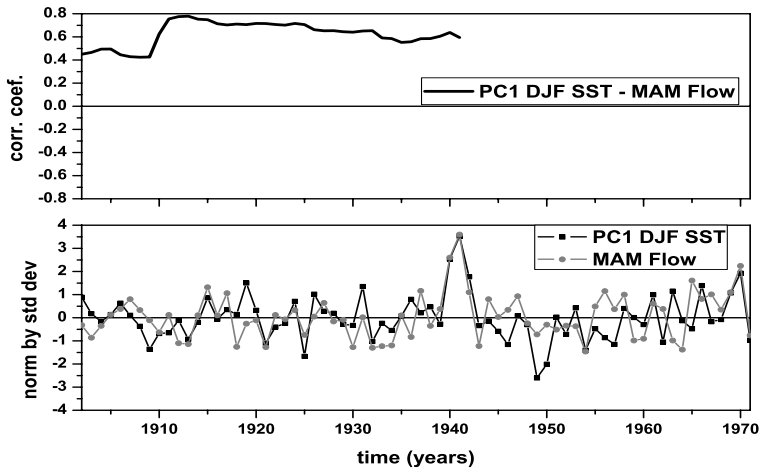

Figure 4. a) The stability map of the correlation between spring flow and winter SST anomalies. Regions where the correlation is stable, positive and significant at 90% (80%) level for at least 80% windows are shaded with red (orange). The corresponding regions where the correlation is stable but negative are shaded with blue (violet). b) First EOF of the SST indices (see Table II for definition). c) Running correlation (31 year window) between spring flow and PC1 of SST indices (upper panel) and spring flow anomalies (grey line) and PC1 (dark line) of winter SST from stable regions.

a)

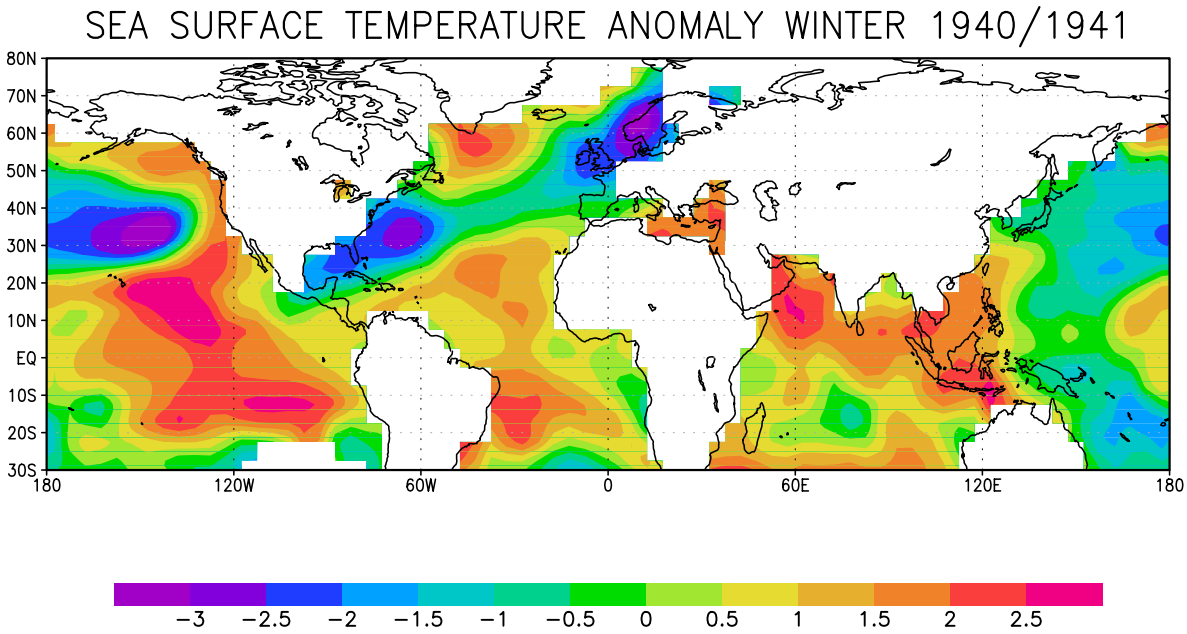

b)

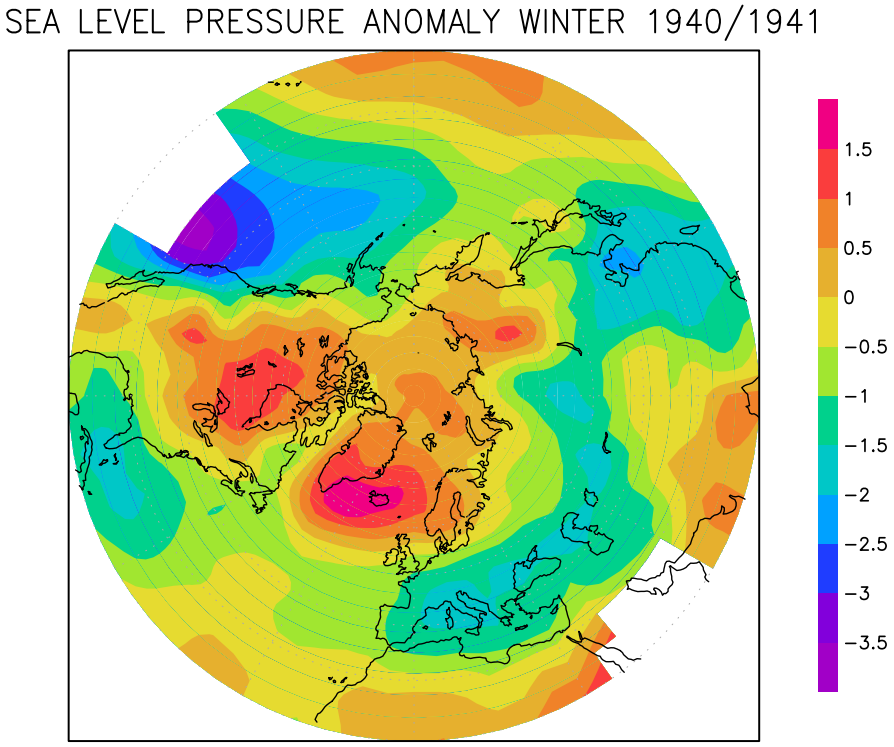

Figure 5. a) Sea surface temperature anomalies and b) sea level pressure anomalies for the winter 1940/41. Units ºC and hPa.

a)

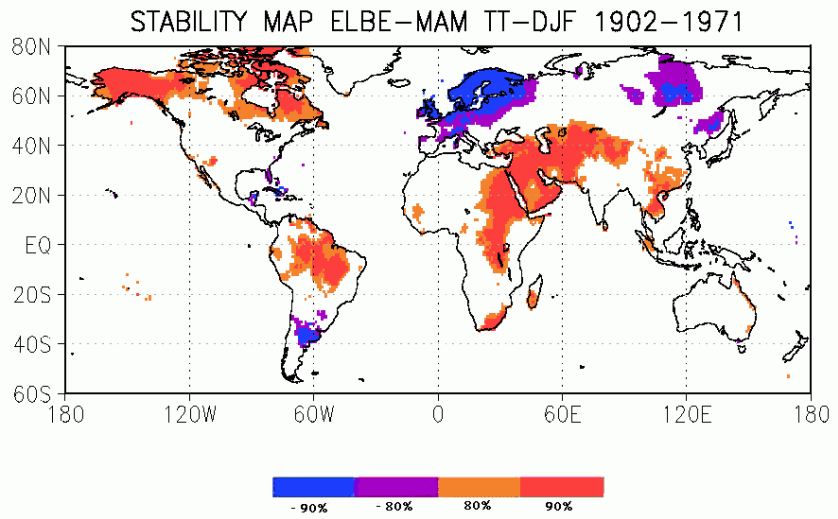

b)

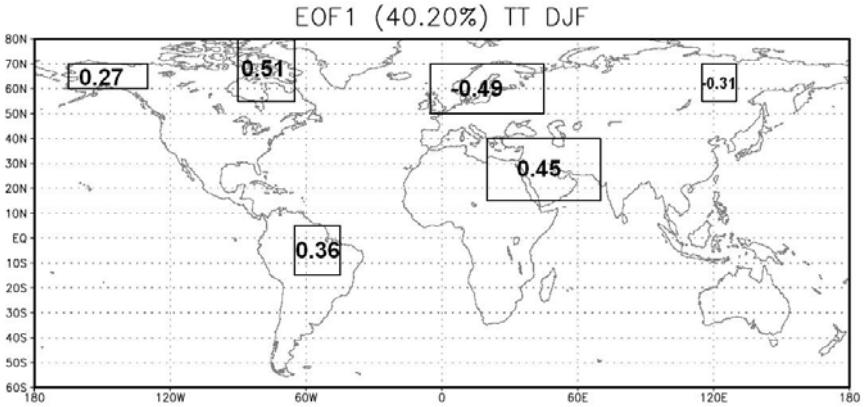

c)

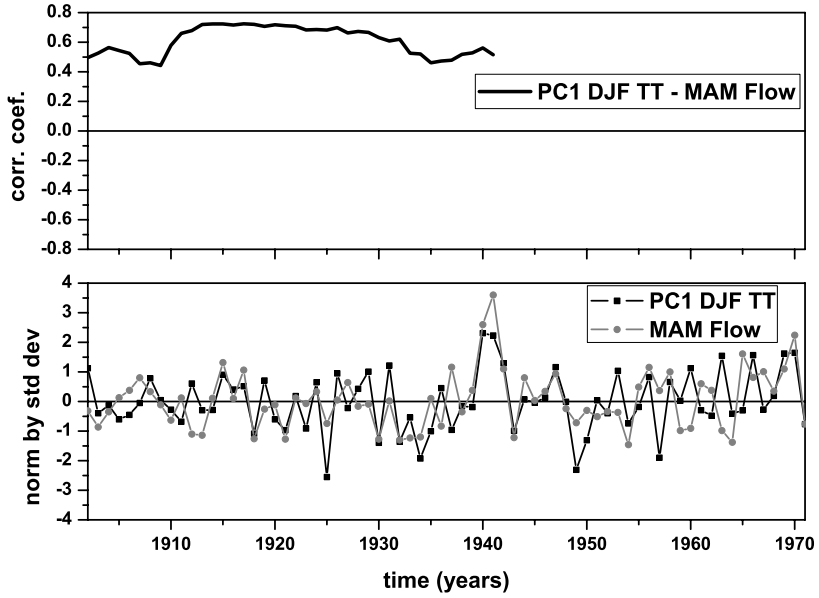

Figure 6. As in figure 4, but for TT

a)

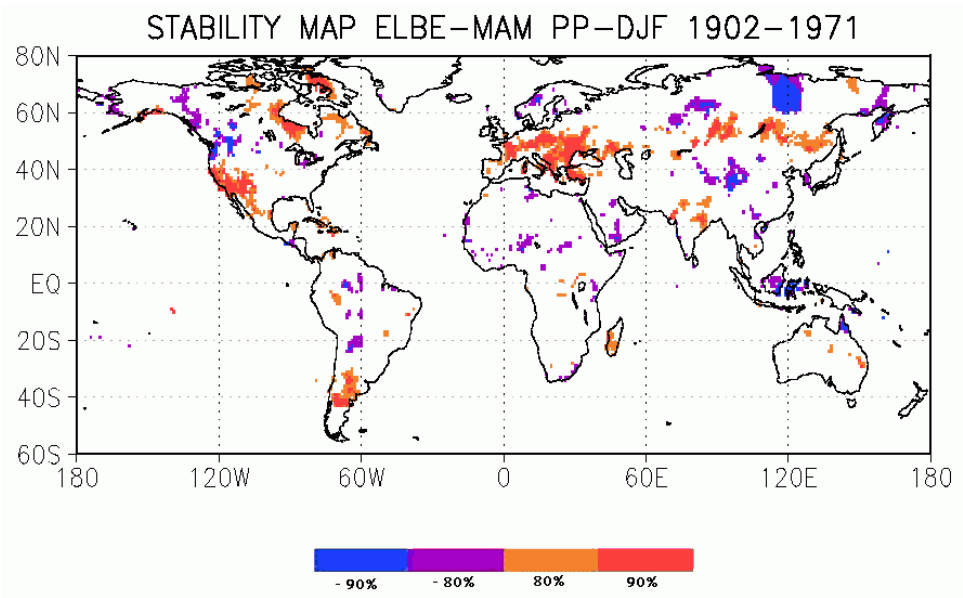

b)

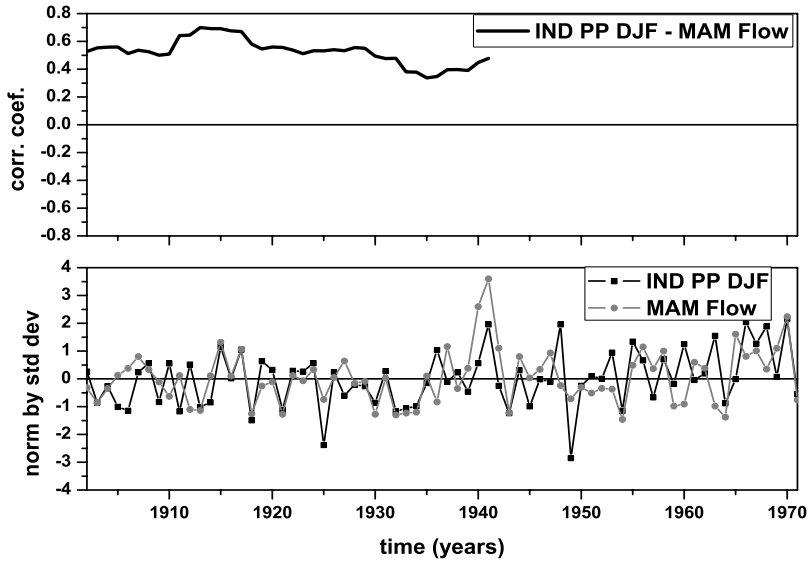

Figure 7. a) The stability map of the correlation between spring flow and winter PP anomalies. Regions with stable correlations are shaded. b) Running correlation (31 year window) between spring flow and PP index (see Table II for definition) (upper panel) and spring flow anomalies (grey line) and winter PP index (dark line) from the stable region.

a)

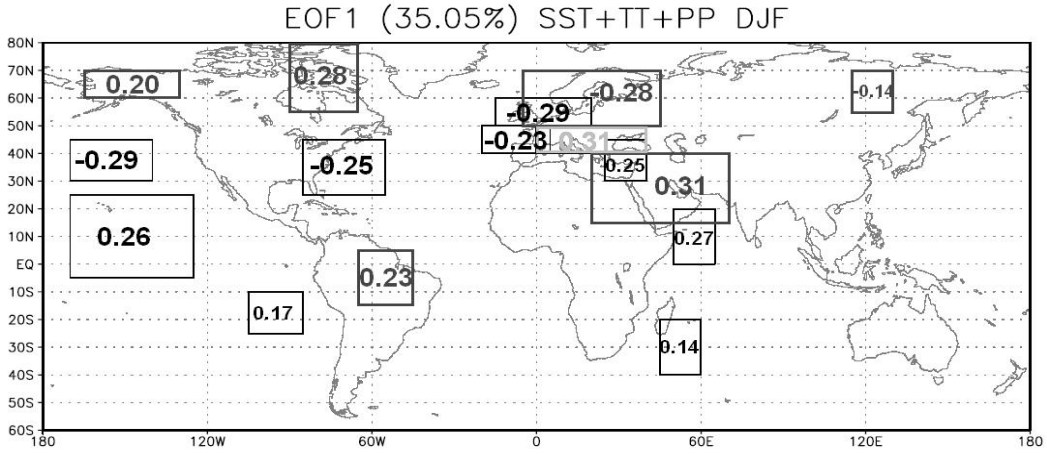

b)

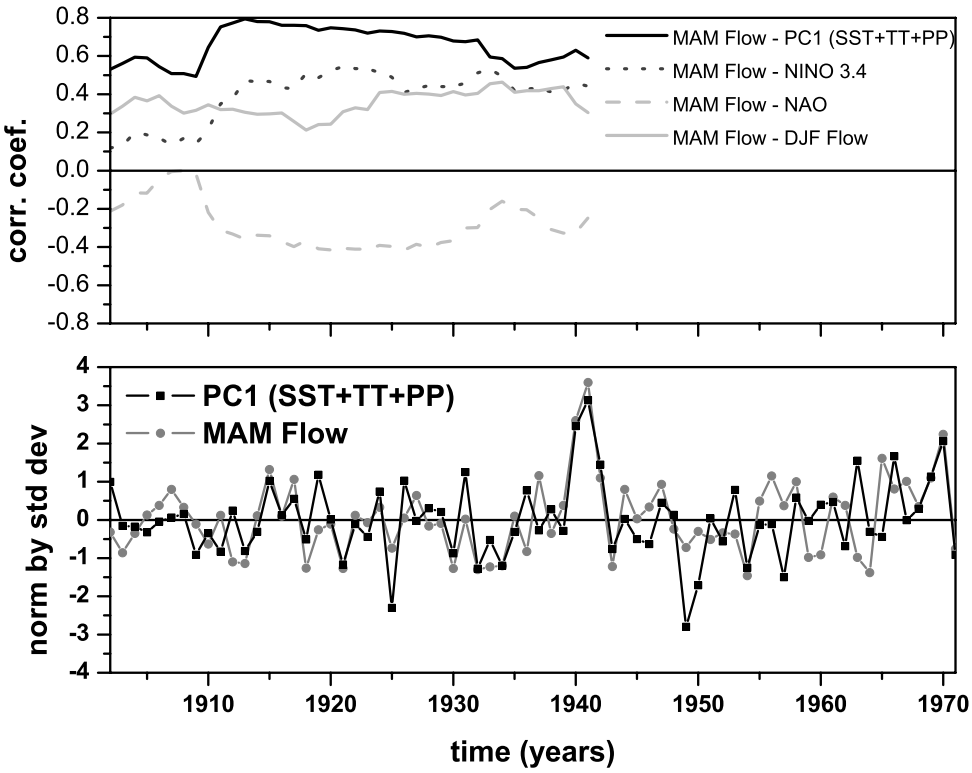

Figure 8. a) First EOF of the (SST+TT+PP) indices identified in Figures 4, 6 and 7 (see Table II for definition). b) Running correlation (31 year window) between spring flow and PC1 of (SST+TT+PP) indices (black line), NAO index (light dashed grey line), Niño3 index (dark dotted grey line) and winter flow anomalies (light grey line)[upper graph] and the time series of PC1 (dark line) of winter (SST+TT+PP) from the stable regions and spring flow anomalies (grey line)[lower graph].

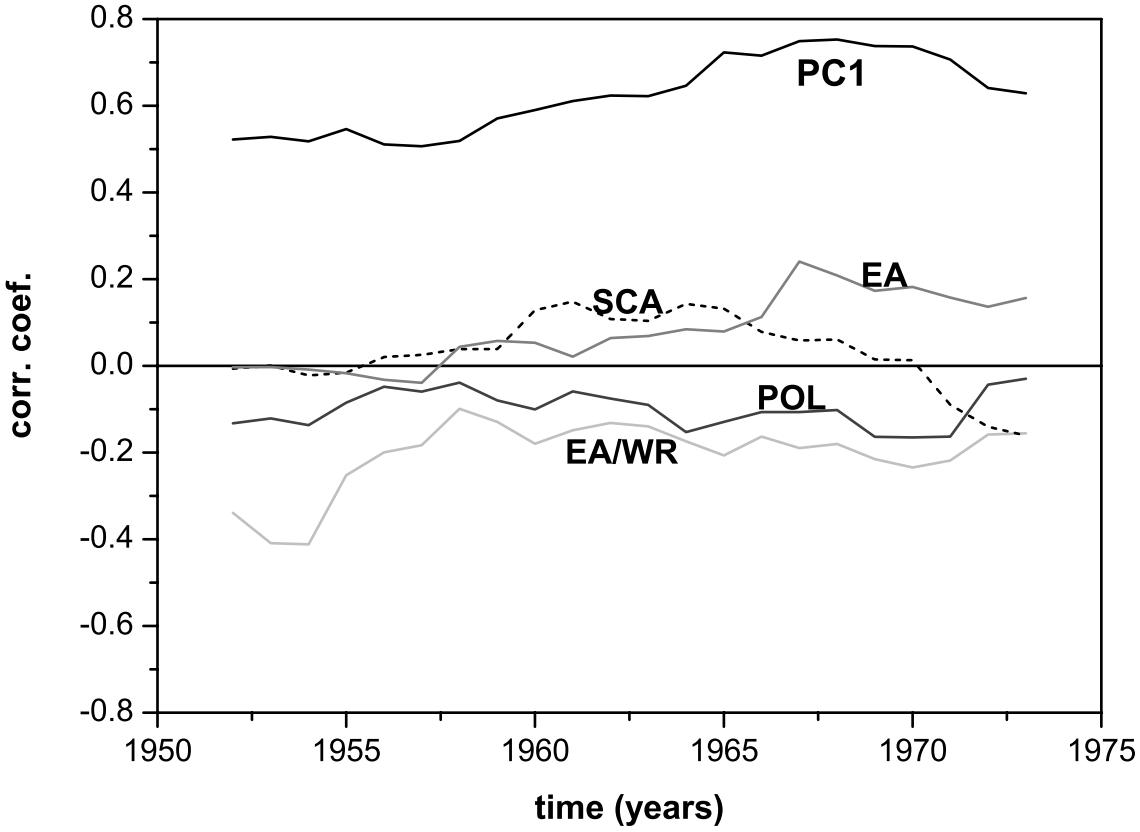

Figure 9. Running correlation (31 year window) between spring flow and teleconnection indices from the North Atlantic region (see Table I for details).

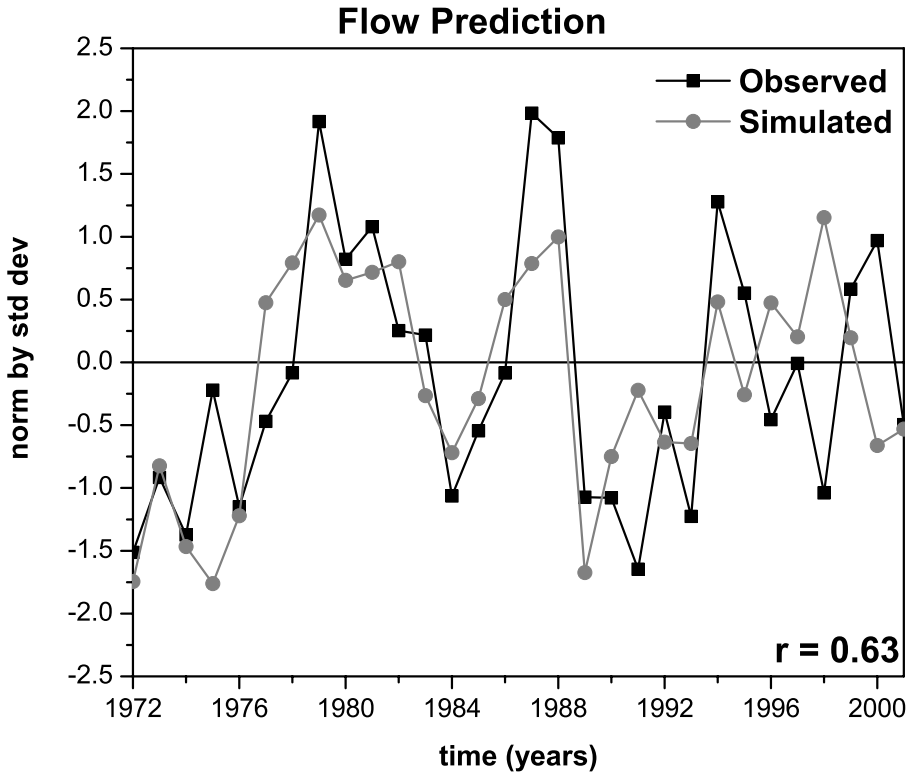

Figure 10. Observed (back line) and predicted (grey line) spring flow anomalies for the period 1972-2001 based on winter (SST+TT+PP) anomalies from the stable regions.

Table I. Teleconnection indices used in this study, time period and their source

Name	**Explanation**	**Period**	**Data source**
EA	East Atlantic	1950-2001	http://www.cpc.noaa.gov/data/teledoc/ea.shtml
EA/WR	East Atlantic/Western Russia	1950-2001	http://www.cpc.noaa.gov/data/teledoc/eawruss.shtml
NAO	North Atlantic Oscillation	1902-2001	http://www.cru.uea.ac.uk/cru/data/nao.htm
NINO 3.4		1902-2001	http://ingrid.ldgo.columbia.edu/SOURCES/.Indices/.nino/.KAPLAN/
POL	Polar/Eurasia	1950-2001	http://www.cpc.noaa.gov/data/teledoc/poleur.shtml
SCA	Scandinavia	1950-2001	http://www.cpc.noaa.gov/data/teledoc/scand.shtml

Table II. The coordinates (latitude, longitude) of the winter SST, TT and PP indices used in this study

SST	TT	PP
170.5ºW-125ºW; 5.5ºS-25.5ºN	65.5ºW-45.5ºW; 15.5ºS-5.5ºN	0.5ºE-45.5ºE; 40.5ºN-50.5ºN
170.5ºW-140ºW; 30.5ºN-45.5ºN	165.5ºW-130.5ºW; 60.5ºN-70.5ºN	
85.5ºW-55ºW; 25.5ºN-45.5ºN	90.5ºW-65ºW; 50.5ºN-80.5ºN	
20.5ºW-5ºE; 40.5ºN-50.5ºN	5.5ºW-45.5ºE; 50.5ºN-70.5ºN	
15.5ºW-20ºE; 50.5ºN-60.5ºN	20.5ºE-70.5ºE; 15.5ºN-40.5ºN	
50.5ºE-65ºE; 0.5ºN-20.5ºN	115.5ºE-130.5ºE; 55.5ºN-70.5ºN	
45.5ºE-60ºE; 40.5ºS-20.5ºS		
105.5ºW-85ºW; 25.5ºS-10.5ºS		
25.5ºE-40.5ºE; 30.5ºN-45.5ºN		

Table III. Seasonal forecast skill score measured against climatology (second column) and against persistence (third column)

Predictand	S_{clim}	S_{pers}
PC1 (SST+TT+PP)	0.20	0.21
NAO	-0.51	-0.49
NINO	-0.28	-0.27